Solution-Processed, Barrier-Confined, and 1D Nanostructure Supported Quasi-quantum Well with Large Photoluminescence Enhancement

Keyou Yan,[†] Lixia Zhang,[‡] Qin Kuang,[†] Zhanhua Wei,[†] Ya Yi,[‡] Jiannong Wang,[‡] and Shihe Yang*[,†]

[†]Nano Science and Technology Program, Department of Chemistry, and [‡]Department of Physics, William Mong Institute of Nano Science and Technology, The Hong Kong University of Science and Technology, Clear Water Bay, Kowloon, Hong Kong

ABSTRACT Planar substrate supported semiconductor quantum well (QW) structures are not amenable to manipulation in miniature devices, while free-standing QW nanostructures, *e.g.*, ultrathin nanosheets and nanoribbons, suffer from mechanical and environmental instability. Therefore, it is tempting to fashion high-quality QW structures on anisotropic and mechanically robust supporting nanostructures such as nanowires and nanoplates. Herein, we report a solution quasi-heteroepitaxial route for growing a barrier-confined quasi-QW structure (ZnSe/CdSe/ZnSe) on the supporting arms of ZnO nanotetrapods, which have a 1D nanowire structure, through the combination of ion exchange and successive deposition assembly. This resulted in highly crystalline and highly oriented quasi-QWs along the whole axial direction of the arms of the nanotetrapod because a transition buffer layer ($Zn_xCd_{1-x}Se$) was formed and in turn reduced the lattice mismatch and surface defects. Significantly, such a barrier-confined QW emits excitonic light ~17 times stronger than the heterojunction (HJ)-type structure (ZnSe/CdSe, HJ) at the single-particle level. Time-resolved photoluminescence from ensemble QWs exhibits a lifetime of 10 ns, contrasting sharply with ~300 ps for the control HJ sample. Single-particle PL and Raman spectra suggest that the barrier layer of QW has completely removed the surface trap states on the HJ and restored or upgraded the photoelectric properties of the semiconductor layer. Therefore, this deliberate heteroepitaxial growth protocol on the supporting nanotetrapod has realized a several micrometer long QW structure with high mechanical robustness and high photoelectric quality. We envision that such QWs integrated on 1D nanostructures will largely improve the performance of solar cells and bioprobes, among others.

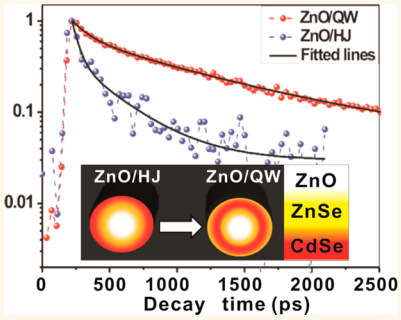

KEYWORDS: organic solution heteroepitaxy · ZnSe/CdSe/ZnSe quantum well · ZnO nanotetrapods · enhanced photoluminescence

Semiconductor quantum well (QW) structure is fundamentally interesting due primarily to quantum confined carriers, facilitated charge transport, prolonged lifetime of fluorescence, and decelerated electron cooling, lending the potential for their integration in nanophotonics and nanoelectronics.[1−6] In principle, high-quality QW structures can be produced by molecular beam epitaxy and metal organic chemical vapor deposition on planar substrates, but the methods are costly and instrument intensive and, more importantly, are intractable to nanoscale manipulation and integration in miniature devices on a large scale.[7−16] In recent years, cheap and facile solution processes have been developed for fabricating soft and flexible size-confined 2D entities such as nanoplates and nanoribbons *via* strongly anisotropic growth, opening the way for solution-processable QWs on the nanoscale.[17−23] However, the scrolling and crumpling tendency of large-sized soft and colloidal QWs limits their cutting-edge applications.[24]

On the other hand, nanorods and nanowires have been widely used in miniature electronics, even for biosensing and endoscopy, because their one-dimensional (1D) morphology and structural robustness permit easy mechanical manipulation, assembly, and integration.[25−36] Such anisotropic nanostructures, when integrated with the QW genre, could underlie a wide range of applications that leverage their unique photonic, spintronic, and optomechanic properties. Therefore, by accreting a QW structure on a 1D supporting structure such

* Address correspondence to chsyang@ust.hk.

Received for review January 24, 2014 and accepted February 28, 2014.

Published online March 01, 2014
10.1021/nn500465w

as nanowires will not only make headway in nanoscale fabrication but also add novel and often critical properties to photonic and photovoltaic devices.

Recently, by using a low-temperature (40−50 °C) aqueous solution approach, we developed a quasi-QW structure on ZnO nanotetrapods, which served as the mechanical support as well as the nanoscale substrate of heteroepitaxial growth. The use of such a novel QW structure in semiconductor-sensitized solar cells has allowed us to achieve a record efficiency.[37] In that study, however, we failed to detect photoluminescence (PL) from the active sensitizer material, *e.g.*, CdSe, which prevented us from probing deeper into the photoinduced charge separation, charge transport, and recombination processes. Most probably, the absence of PL from CdSe was a result of the aqueous synthesis at a relatively low temperature, which could give rise to low crystallinity and numerous defects. Therefore, a higher temperature synthesis could solve this problem and could more dramatically enhance the solar cell efficiency.

In the present work, we demonstrate an organic solution based successive deposition approach at much higher temperatures for quasi-heteroepitaxial growth of a barrier-confined 2D quantum structure (ZnSe/CdSe/ZnSe) on a 1D supporting nanotetrapod. A key step is to introduce a transition layer ($Zn_xCd_{1-x}Se$) with a graded composition at the interface to reduce lattice mismatch between ZnSe and CdSe, which yielded quasi-QWs with single crystallinity in local areas and highly aligned along the entire arms of the ZnO tetrapods. Significantly, strong PL of CdSe from the QWs could be observed even with the naked eye. More precisely, we found that typical ZnSe/CdSe/ZnSe sandwiched QWs on ZnO nanotetrapod arms (ZnO/QW) exhibit excitonic PL ∼17 times stronger than the ZnSe/CdSe heterojunction (HJ) counterpart at the single-particle level. When formed into a film, the former still shows more than 10 times stronger PL than the latter. Time-resolved photoluminescence from ensemble QWs exhibits a lifetime of up to 10 ns, contrasting sharply with ∼300 ps for the control HJ sample. Such a dramatic PL enhancement can be attributed to the removal of the surface trap states of CdSe by the ZnSe layer, which is supported by our single-particle PL and Raman studies. Therefore, the deliberate heteroepitaxial growth on the supporting nanotetrapod has achieved ultralong length, high mechanical robustness, and high quality of the QW structure, bringing potential applications in solar cell and bioprobe devices.

RESULTS AND DISCUSSION

The vapor-phase synthesis of ZnO tetrapods has been reported previously,[38] which are morphologically similar to the metal chalcogenide tetrapods synthesized in solution growing out from similar thermodynamic and kinetic control.[39−41] In general, the as-prepared ZnO tetrapods we synthesized (see Figure S1 (left) and Figure S2) display a smooth backbone surface, which is typically matte after QW assembly thereon (see Figure S1 (right)).

Figure 1 establishes the formation of the ZnSe/CdSe/ZnSe QW structure on ZnO tetrapods by ion exchange and subsequent successive injection of precursors. Shown in Figure 1A is the synthesis procedure of the QW structure, while Figure 1B presents the resultant structures after each step. Since the oxygen atoms on the ZnO surface could be facilely replaced by the highly active Se in octadecene (ODE) solution (Se-ODE) at high temperatures, the ion exchange in step I yielded a stable ZnSe shell about 5 nm thick, forming a core/shell tetrapod with a $ZnSe_xO_{1-x}$ transition interface (labeled as ZnO/ZnSe). Actually, compared to the previously reported aqueous approach,[37] the replacement rate (2−3 nm/h) in the organic solution is lower, judging from the delayed appearance of the yellowish color of ZnSe, thereby resulting in a more close-fitting shell. From the corresponding TEM images, one can observe that the smooth surface of the ZnO tetrapod (see Figure 1(B1)) becames matte after the surface selenylation (Figure 1(B2)). Lattice fringe changes can be distinguished from the HRTEM images in Figure 1(C1) and (C2). Figure 1(C1) displays continuous and complete ZnO (0001) facets from the core to the lateral surface of a nanorod, whereas Figure 1(C2) features a transition region from the ZnO lattice to the ZnSe lattice, which is roughly separated by a dashed white line to guide the eye. After transferring the ZnO/ZnSe powder to a 25 mL ODE solution, reactive precursors were successively injected. Different from the previous successive deposition approaches,[42−47] our synthetic route was intended to minimize the use of ligand surfactants and thus the etching of the host ZnO tetrapod, keeping the ZnO/QW mechanically stable. In step II, the CdSe shell growth was continued through the successive injection of 0.5 mL of Cd-OA precursor and 0.5 mL of Se-ODE precursor for four cycles (the sample is labeled as ZnO/HJ and shown in Figure 1(A3)), each cycle yielding a *ca.* 2−2.5 nm thick shell (see the TEM image in Figure 2). After completing this step, a thicker shell of CdSe was deposited at the outmost surface, forming peninsula-like features induced by surface strain (see Figure 1(B3 and C3)). In step III, through successive injection of 0.5 mL of Zn-OA precursor and 0.5 mL of Se-ODE precursor for four cycles, the outermost ZnSe shell was formed (shortened as ZnO/QW and schematized in Figure 1(A4)). Figure 1(B4) gives TEM images of the ZnO/QW structure, while Figure 1(C4) depicts the final structure around the interface between QW and ZnO.

In order to more clearly elucidate the structures of the HJ and QW, the ZnO cores were removed with acetic acid, leaving behind only the HJ and QW nanotubes for easy observation. Figure 2A−D display an HJ

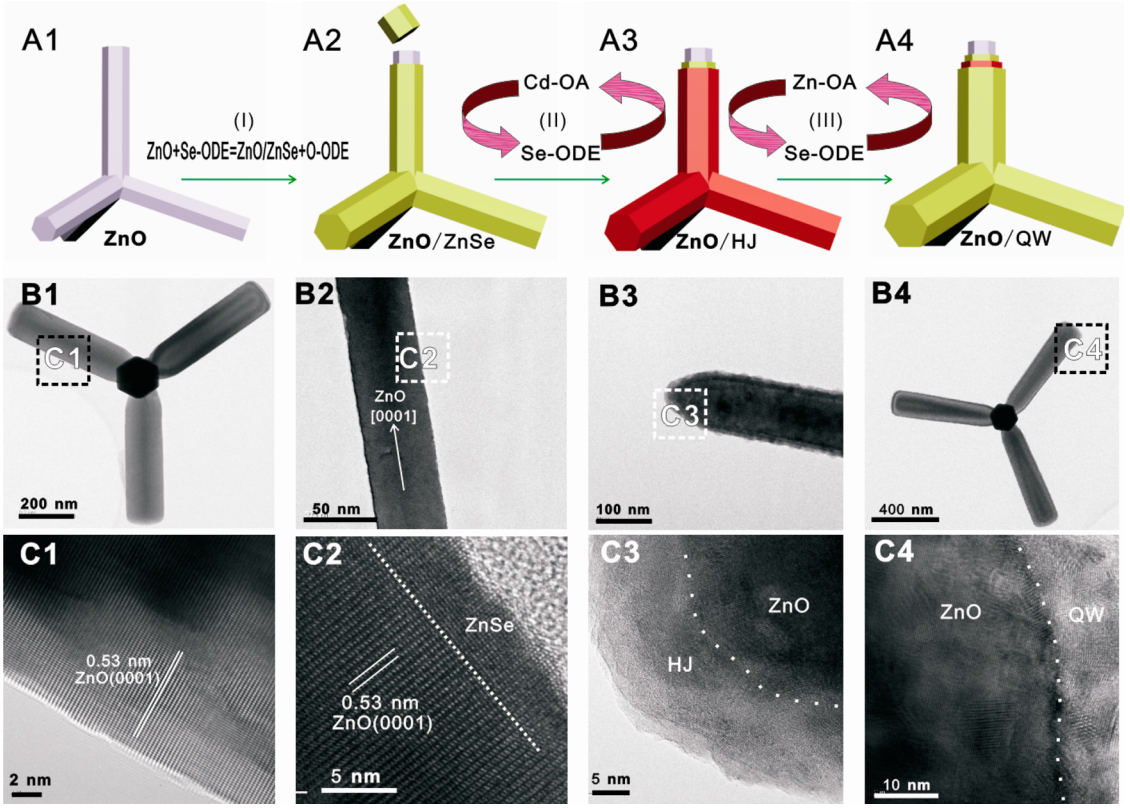

Figure 1. Organic solution processed heteroepitaxy on ZnO tetrapods. (A) Schematic illustration of solution process steps; (B) TEM images of the nanostructures formed from each step; (C) HRTEM images of the nanostructures formed from each step.

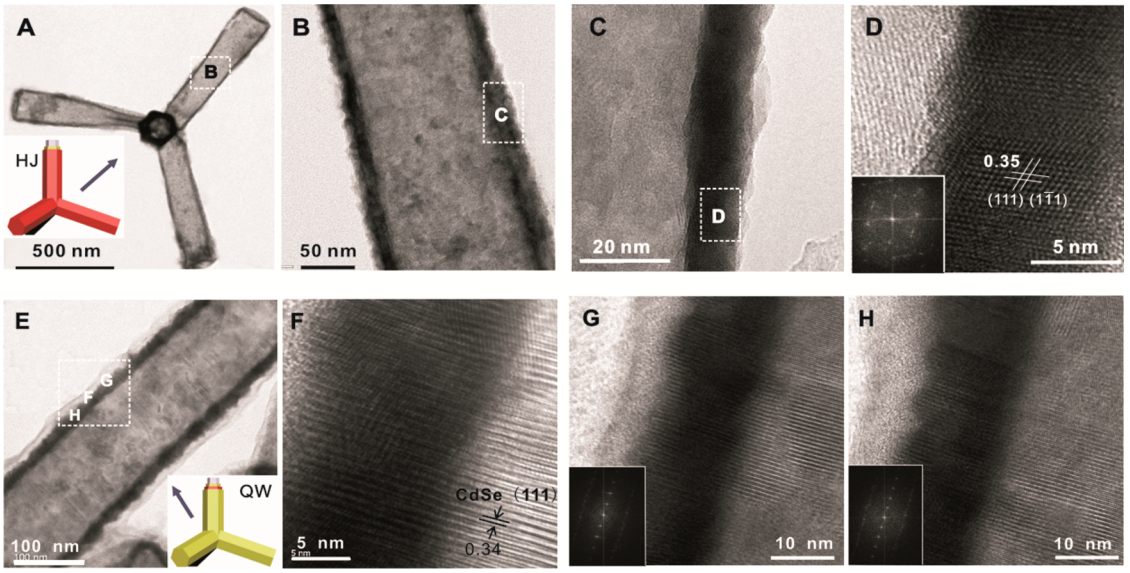

Figure 2. Detailed views of the HJ and QW after removal of ZnO in ZnO/HJ and ZnO/QW: (A) TEM image of an HJ tetrapod tube; (B) TEM image of one of the HJ tetrapod arms; (C) close-up of the region enclosed by the dashed-line rectangle in (B); (D) HRTEM image of the HJ tube shell (inset is the corresponding FFT pattern); (E) TEM image of one of the arm tubes of a QW tetrapod tube (the framed area is separately shown in (F), (G), and (H) in an enlarged view); (F) zoom-in HRTEM image of the "F" spot in the QW arm tube shell indicated in (E); (G) zoom-in HRTEM image of the "G" spot in the QW arm tube shell indicated in (E) and the corresponding FFT pattern (inset); (H) zoom-in HRTEM image of the "G" spot in the QW arm tube shell indicated in (E) and the corresponding FFT pattern (inset).

nanotube tetrapod viewed from the top structures through one of the four nanotubes and a close-up of a tubular arm, the shell of the arm, to the bottom lattice fringes of the tube shell. In general, the HJ is highly crystalline at least on a small scale. However, we notice that the outer surface of the HJ tube is coarse as a

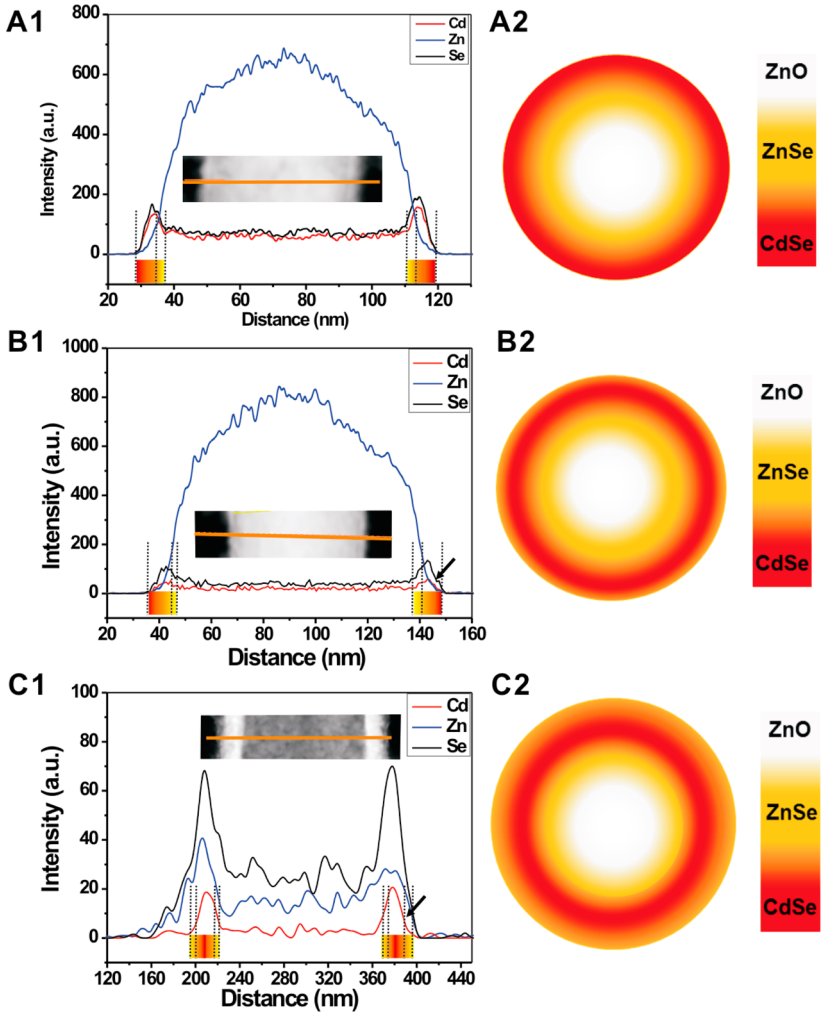

Figure 3. EDS line scan profiles of the sensitizer structure: (A1, 2) STEM image (inset) and EDS line-scan analysis of a ZnO/HJ (ZnSe/CdSe/ZnSe(0 cycle)) and cross-sectional illustration of a HJ tube; (B1, 2) STEM image (inset) and EDS line-scan analysis of a transition structure from ZnO/HJ toward ZnO/QW (ZnSe/CdSe/ZnSe(2 cycles)) and cross-sectional illustration of an evolving tube highlighting the transition structure from ZnO/HJ to ZnO/QW; (C1, 2) STEM image (inset) and EDS line-scan analysis of a final complete QW nanotube (ZnSe/CdSe/ZnSe(4 cycles)) and cross-sectional illustration of a QW tube. Blue dashed lines are a guide to the eye to distinguish the domains of CdSe and ZnSe: red and yellow squares denote CdSe and ZnSe, respectively.

whole, which can be explained by the lattice mismatch (7.4%) induced by the step of sequential deposition of CdSe onto ZnO/ZnSe. Figure 2E−H show fine details of a final QW nanotube structure. The distinct, straight lattice fringes in Figure 2F, G, H and the corresponding FFT patterns in the insets suggest that the shell is highly crystalline or single crystalline within a local area, and overall, it is highly oriented as well. This is a desirable feature for optimizing the 2D QW electronic structure. Through comparison, one can observe that the matte surface of the HJ tubes is rectified and becomes smooth after the final deposition of ZnSe, suggesting void filling by ZnSe coating and alloying with CdSe, which greatly relieve the lattice mismatch strain and thus yield the highly aligned QW structure.

To clarify the lattice rectification process from the HJ to the QW, we closely examined the successive deposition process by EDX line scan. A control sample with only two cycles of final ZnSe coating was also tested, and its TEM images are shown in Figures S3−7 (denoted as ZnSe/CdSe/ZnSe(2 cycles)). For ZnO/HJ, from Figure 3(A1), we can see that the HJ structure is clearly made of the inner ZnSe-rich shell and the outer CdSe-rich shell, with a composition graded layer between them resulting from the Kirkendall effect,[48] which is schematically illustrated as a color transition from yellow to red in Figure Figure 3(A2). After two cycles of ZnSe coating, one can find that the shell is not the well-defined ZnSe-rich shell around the outermost surface as expected (see Figure 3(B1, 2)), but rather an alloy of $Zn_xCd_{1-x}Se$ as schematized in Figure 3(B2), conforming to the elemental distribution in Figure 3(B1). This hints at an ion exchange and alloying step in the successive deposition process, which results in a radially composition graded region. In other words, the first two cycles did not really yield a much thicker shell (only 1−2 nm thick) but instead transformed as thick as about 5 nm of the outermost CdSe to the composition

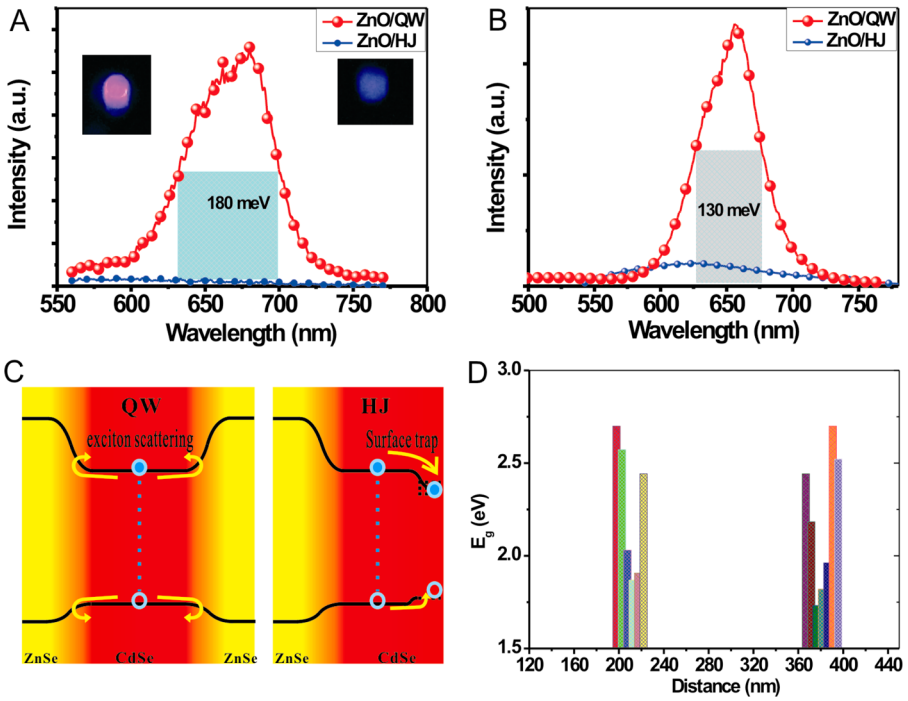

Figure 4. Steady-state PL spectra of ZnO/HJ and ZnO/QW. (A) Room-temperature PL spectra (left inset: photoimage of ZnO/QW under 400 nm excitation; right inset: photoimage of ZnO/HJ under 400 nm excitation; (B) 17 K PL spectra; (C) schematic illustration of exciton scattering and confinement in QW (left) and exciton trapping to surface traps in HJ (right); (D) band gap profile of the QW structure in Figure 3C obtained from the nonlinear bowling equation (see SI).

graded layer (see arrows in Figure 3B and C). It turns out that the alloying step actually forms a transition region between the CdSe-rich shell and the ensuing ZnSe-rich shell and helps to rectify the bottom lattice and the top morphology,[40,41] thereby yielding the high-quality QW structure. Indeed, after another two cycles of ZnSe coating (denoted as ZnSe/CdSe/ZnSe(4 cycles)), an outermost ZnSe-rich shell (about 2.5 nm/cycle) is finally added, as can be seen from Figure 3(C1), which sandwiches the CdSe QW together with the inner ZnSe shell (see Figure 3(C2)).

In view of its potential appealing photoelectric properties, such a barrier-confined QW structure was subjected to PL studies. First, we comparatively measured the PL of the two films made of ZnO/HJ and ZnO/QW at room temperature and low temperature. After 400 nm laser excitation, we could observe the emitted red light from ZnO/QW through the naked eye, but no emitted colored light was observed from ZnO/HJ (see inset). Figure 4 shows the PL spectra at room temperature (A) and at 17 K (B). First, one can observe that the PL peak at 17 K is much narrower than that of room temperature (fwhm ~130 meV *vs* 180 meV), which can be attributed to the suppression of phonon oscillation and Auger recombination at the low temperature.[49] Second, ZnO/QW displays distinctly stronger PL (by more than an order of magnitude) than ZnO/HJ. Finally, the PL from ZnO/QW is red-shifted from that of ZnO/HJ, and this is probably due to the size increase and void filling during the coating of the final ZnSe shell. As to the much more intense PL of ZnO/QW, the localized exciton effect may be the explanation. In such a barrier-confined ZnO/QW structure, both electrons and holes stemming from photoexcitation are presumably confined in the smooth potential well because of the graded composition interfaces. Figure 4C (left) schematically illustrates such confinement arising from the exciton scattering and confinement, which is similar to the behavior of excitons in core/shell nanostructures.[50] On the contrary, the HJ structure is riddled with surface states of CdSe, which could act as trap centers for dissociating excitons and thereby quenching the PL as we observed (see Figure 4C, right).[51] In order to manifest the band structure of QW, the energy band gap profiles have been approximately deduced based on Figure 3C with a bowling factor of 0.67 and are shown in Figure 4D (see the SI).[37,52,53] The potential well revealed in Figure 4D supports the presumed barrier confinement in the QW structure.

More carrier dynamic information was obtained from the TRPL measurements on the two structures. Figure 5A and B display the TRPL mapping images across the visible wavelength range taken by the streak camera. Several features are noteworthy. First, ZnO/QW exhibits 17 times stronger PL and a much sharper emission band than ZnO/HJ, which is consistent with the steady-state PL results described above and the single-particle PL spectra in Figure 5D. Second, more importantly, the PL decay trace of ZnO/QW displays a

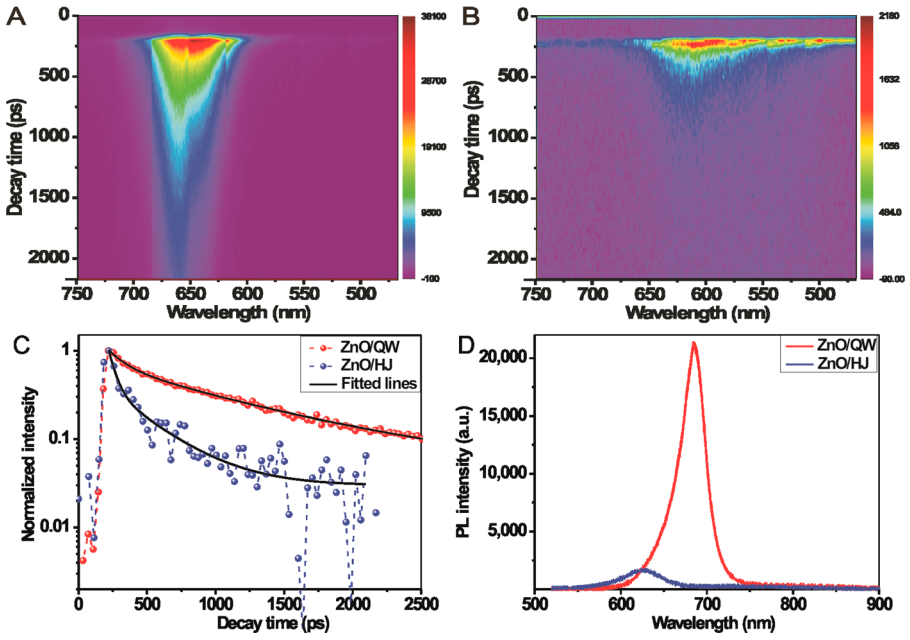

Figure 5. Time-resolved PL spectra and single-particle PL spectra of ZnO/HJ and ZnO/QW. (A) TRPL mapping image of ZnO/QW; (B) TRPL mapping image of ZnO/HJ; (C) PL decay traces of ZnO/QW and ZnO/HJ; (D) single-particle PL spectra of ZnO/QW and ZnO/HJ.

TABLE 1. TRPL Decay Times Obtained from the Fitting of the TRPL Data for the ZnO/HJ and ZnO/QW Samples

sample	τ_1 (ps)	A_1%	τ_2 (ps)	A_2%	τ_3 (ps)	A_3%
ZnO/HJ	332.4	1.1%	48.9	98.9%		
ZnO/QW	10675.4	8.0%	824.7	23.4%	121.0	68.6%

much longer and narrower comet-like tail extending to as long as several nanoseconds, whereas that of ZnO/HJ drops quickly, yielding a much shorter lifetime. Figure 5C directly compares the decay traces of ZnO/QW and ZnO/HJ. In general, the excited ZnO/QW displays a typical triexponential decay with time, whereas the decay trace of ZnO/HJ shows a biexponential form. We have quantitatively extracted the decay lifetimes, which are listed in Table 1. Remarkably, the extraction lifetimes are as long as 10675.4, 824.7, and 120.9 ps for the three decay components of the ZnO/QW film but only 332.5 and 48.9 ps for the two decay components of the ZnO/HJ film. The much longer lifetime of ZnO/QW can be attributed to the much fewer surface traps, which act as charge acceptors that dissociate excitons and therefore reduce the photoluminescence of ZnO/HJ.[51] The different decay components arise from the dynamic processes of excitons and carriers in the system.[54−56] From the differences of the structure and band gap profile between ZnO/QW and ZnO/HJ described above, the three decay components of the ZnO/QW in the order of short to long lifetimes are probably ascribable to charge transfer along the axial direction, charge transfer to surface traps, and band-edge recombination, while for the two decay components of the ZnO/HJ film, only charge transfer to surface traps and band-edge recombination are retained. Charge transfer can shorten the lifetime since it directly dissociates excitons and quenches the PL.[51] The charge transfer along the axial direction is activated in ZnO/QW because of the piping effect in the barrier-confined QW and the elastic scattering at the well boundaries, accounting for the fastest quenching component.[37] For charge transfer to surface traps, the pre-exponential fraction decreases from 98.9% for ZnO/HJ to 23.4% for ZnO/QW, which can be attributed to the reduction of the surface trap states by seamlessly sandwiching the CdSe layer with two ZnSe layers. The charge transfer to surface traps will be further investigated below by single-particle PL and Raman spectroscopy. Finally, the prolonged lifetime of band-edge recombination in ZnO/QW compared to ZnO/HJ can be attributed to the crystalline quality improvement after the rectification step of lattice mismatch, as well as the barrier confinement, which we have described in detail above.

The PL spectra of ZnO/QW and ZnO/HJ have also been studied at the single-particle level, in which the ensemble averaging effects were excluded. In this experiment, the laser beam was focused onto a 1 μm spot at different locations of the nanorod, which is actually an arm of a tetrapod (see Figure 6(A1) and (B1)). Figure 6(A2) and (B2) display the PL spectra of the single nanorod. One can observe that the PL peaks have different fwhm distributions between ZnO/QW and ZnO/HJ. In detail, however, the PL peaks of ZnO/QW have similar and as narrow as about 85 meV fwhm at different locations of the nanorod, whereas those of ZnO/HJ have dispersive and as broad as >140 meV fwhm,

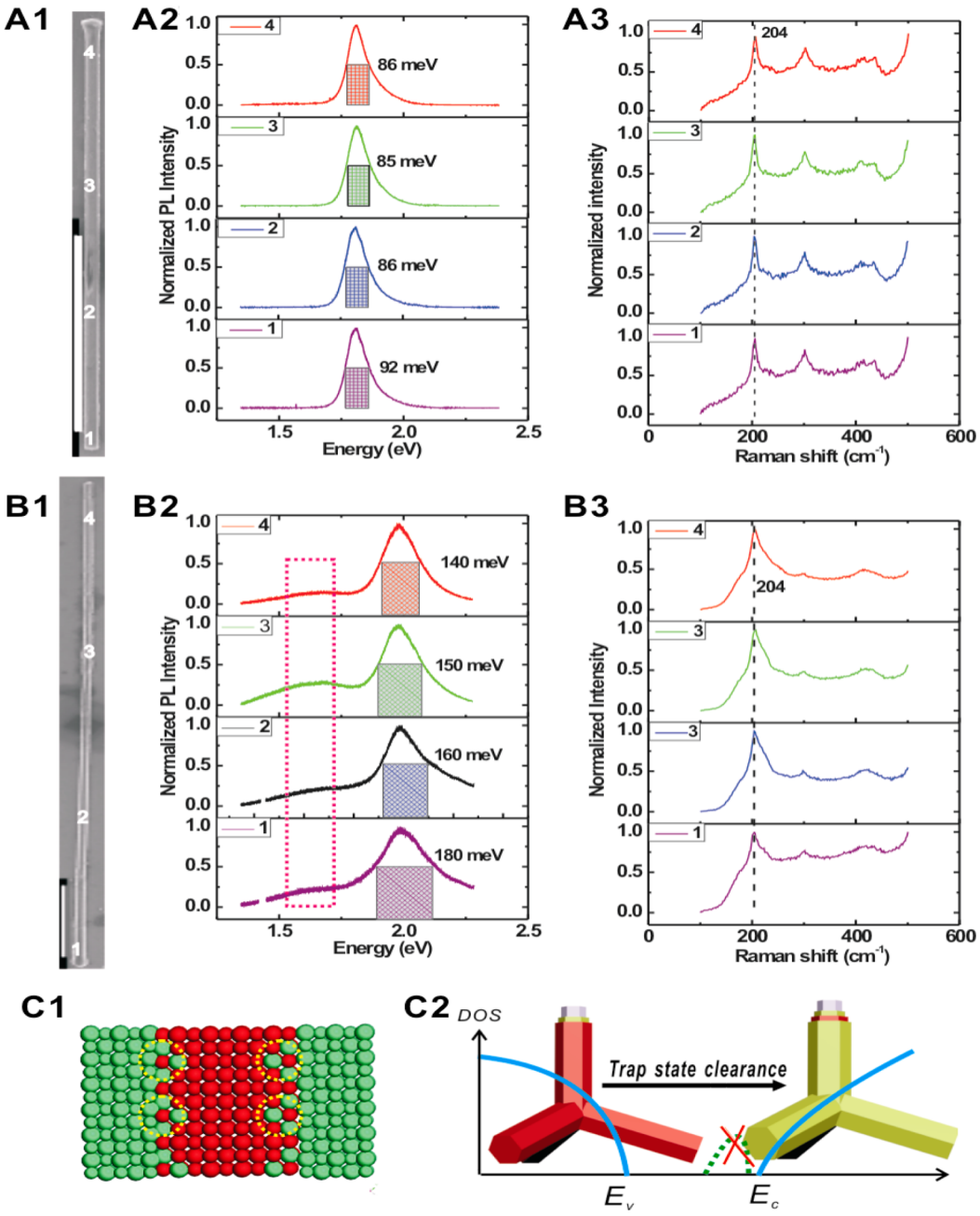

Figure 6. Single-nanorod spectroscopy of ZnO/QW and ZnO/HJ. (A1, 2, 3) SEM image and PL and Raman spectra at different spots of the single ZnO/QW nanorod (of a tetrapod); (B1, 2, 3) SEM image and PL and Raman spectra at different points of the single ZnO/HJ nanorod (of a tetrapod); (C1, 2) schematic illustrating the ZnSe filling of surface trenches on the CdSe layer (left) and the spectral changes due to trap state clearance (right) in the QW. Scale bar: 5 μm.

manifesting the much smaller size dispersity of the former than the latter after the surface rectification. Besides, as shown in Figure 6(B2), the defect PL peak on the red side of the major PL peak can be observed at ~1.6 eV for ZnO/HJ (framed in the dashed rectangle), which can be attributed to the surface defects of HJ. However, such a defect peak is absent for ZnO/QW, suggesting that these energy states of surface defects have been completely removed by the barrier confinement through the final ZnSe coating. Figure 6(A3) and (B3) present the corresponding Raman spectra for the two structures. For both samples, CdSe can be identified by the distinct peak at 204 cm^{-1} arising from its first-order longitudinal optical phonon mode (LO-CdSe), suggesting the existence of CdSe in the structures.[57,58] In spite of the similar spectral positions, distinctively, the Raman peak of ZnO/HJ is much wider than that of ZnO/QW, indicating that ZnO/HJ has a higher and more dispersive density of states than ZnO/QW due to the surface defects, yielding much more electron transition paths after excitation. This feature, together with the PL spectra, shores up the presumption that sandwiching

the CdSe layer with ZnSe shells (QW) is an efficient strategy to ameliorate the PL properties of CdSe in the 2D structure because of the clearance of surface trap states. Figure 6(C1) schematically illustrates the structure of the barrier-confined QW, in which ZnSe is epitaxially grown on the surface of CdSe with a layer of graded compositions. It is through such a passivation step with ZnSe that the surface trap states of the CdSe layer are totally removed (Figure 6(C2)), yielding the high-quality quasi-QW structure. Such a nanowire-supported QW structure, due to the aforementioned long-lived fluorescence imparted, can be probably employed as bioprobes.

CONCLUSION

We have demonstrated an organic solution process to produce a quasi-QW structure (ZnSe/CdSe/ZnSe) on ZnO nanotetrapods and examined the detailed spectroscopic properties of the resulting QW structure with TRPL. This solution process can ensure heteroepitaxy to achieve single crystallinity at local areas and high orientation on the whole nanorod by making a composition-graded transition layer. Single nanorod PL reveals that our quasi-QW has as narrow as 85 meV fwhm and 17 times higher PL intensity than ZnO/HJ at the single-nanorod level. The TRPL study shows that ZnO/QW has a much longer lifetime than ZnO/HJ. This synthesis strategy will provide building blocks of QW accreted on nanowires, thereby integrating the advantageous properties of the QW and the supporting 1D structure. More generally, the incorporation of 2D geometry on a 1D nanowire will bring novel properties desirable for the new generation of bioprobes and photovoltaics.

EXPERIMETAL SECTION

Synthesis of ZnO Tetrapods. ZnO tetrapods were synthesized by the metal vapor transport and oxidation technique we reported previously.[38] Typically, 1 g of Zn strand and a flow of 50/200 O_2/N_2 at standard cubic centimeters per minute (50 sccm/200 sccm) were used in each batch of synthesis, yielding ZnO nanotetrapods with arms of 50−200 nm in diameter and 400 nm to dozens of micrometers in length.

Quasi-heteroepitaxy of QWs on ZnO Tetrapods. The quasi-QWs of ZnSe/CdSe/ZnSe were prepared by successively injecting precursors. First, an appropriate amount (0.1 g) of ZnO tetrapods was placed in a Se-ODE solution (2.0 mg in 50 mL of ODE), which was prepared beforehand by heating Se powder in ODE to above 250 °C under N_2 purging for 2 h, to form 2−5 nm ZnSe shells. The resulting ZnO/ZnSe core/shell tetrapod powder was rinsed with hexane three times and transferred to a 25 mL ODE solution in a 100 mL flask. After heating to 250 °C under N_2 purging, the preprepared 0.5 mL Cd-OA in ODE solution (0.04 M, 0.308 g of CdO was dissolved in 58 mL of ODE + 2 mL of oleic acid (OA) at 280 °C and then was cooled for injection) and 0.5 mL Se-ODE solution (0.04 M, no OA employed) were successively injected every 10 min for four cycles. Similarly, for coating ZnSe under N_2 purging, the preprepared 0.5 mL Zn-OA in ODE solution (0.04 M, 0.204 g was dissolved in 58 mL of ODE + 2 mL of OA at 150 °C and then was cooled for injection) and 0.5 mL Se-ODE solution were successively injected every 10 min for two to four cycles.

Morphology and Spectroscopy Characterization. Morphologies of the nanomaterials and subsequent nanostructures were directly examined with JEOL6700F SEM at an accelerating voltage of 5 kV. TEM observations were carried out on a JEOL 2010F microscope operating at 200 kV. Single-particle PL and Raman measurements were conducted on a Renishaw 2000 laser Raman microscope equipped with a 514.5 nm and 20 mW argon ion laser with a 1 μm spot size for excitation. For TRPL measurements, a tunable Ti:sapphire femtosecond-pulsed laser was used as the excitation light source, with an excitation wavelength of 400 nm and an incident light intensity of 1 W cm^{-2}. A Hamamatsu C5680-04 streak camera was used for the TRPL experiments. The samples were cooled by an APD Cryogenics system (model EXPPANDER DE202), and the TRPL measurements were performed at low temperatures down to 17 K.

Conflict of Interest: The authors declare no competing financial interest.

Acknowledgment. This work was supported by the HK-RGC General Research Funds (GRF No. HKUST 606511, 605710, and 604410).

Supporting Information Available: SEM images of ZnO tetrapods before and after QW assembly, HRTEM images of ZnO tetrapods, TEM images of transition structure ZnSe/CdSe/ZnSe-(2 cycles), and HRTEM images of transition structure ZnSe/CdSe/ZnSe(2 cycles) near the side shell, inside the tube, at the corner, and at the tip. This material is available free of charge *via* the Internet at http://pubs.acs.org.

REFERENCES AND NOTES

1. Hu, Y. J.; Kuemmeth, F.; Lieber, C. M.; Marcus, C. M. Hole Spin Relaxation in Ge-Si Core-Shell Nanowire Qubits. *Nat. Nanotechnol.* **2012**, *7*, 47–50.
2. Kong, D. S.; Koski, K. J.; Cha, J. J.; Hong, S. S.; Cui, Y. Ambipolar Field Effect in Sb-Doped Bi_2Se_3 Nanoplates by Solvothermal Synthesis. *Nano Lett.* **2013**, *13*, 632–636.
3. Koski, K. J.; Cha, J. J.; Reed, B. W.; Wessells, C. D.; Kong, D. S.; Cui, Y. High-Density Chemical Intercalation of Zero-Valent Copper into Bi_2Se_3 Nanoribbons. *J. Am. Chem. Soc.* **2012**, *134*, 7584–7587.
4. Koralek, J. D.; Weber, C. P.; Orenstein, J.; Bernevig, B. A.; Zhang, S. C.; Mack, S.; Awschalom, D. D. Emergence of the Persistent Spin Helix in Semiconductor Quantum Wells. *Nature* **2009**, *458*, 610–613.
5. Stern, N. P.; Myers, R. C.; Poggio, M.; Gossard, A. C.; Awschalom, D. D. Confinement Engineering of s-d Exchange Interactions in $Ga_{1-x}Mn_xAs/Al_yGa_{1-y}As$ Quantum Wells. *Phys. Rev. B* **2007**, *75*, 045329.
6. Crooker, S. A.; Baumberg, J. J.; Flack, F.; Samarth, N.; Awschalom, D. D. Terahertz Spin Precession and Coherent Transfer of Angular Momenta in Magnetic Quantum Wells. *Phys. Rev. Lett.* **1996**, *77*, 2814–2817.
7. Wan, L.; Duan, X. F.; Chen, H.; Liu, H. F.; Li, Z. Q.; Huang, Q.; Zhou, J. M. Transmission Electron Microscopy Study of Hexagonal GaN Film Grown on GaAs (001) Substrate by Using AlAs Nucleation Layer. *J. Cryst. Growth.* **2000**, *220*, 379–383.
8. Aballe, L.; Rogero, C.; Kratzer, P.; Gokhale, S.; Horn, K. Probing Interface Electronic Structure with Overlayer Quantum-Well Resonances: Al/Si(111). *Phys. Rev. Lett.* **2001**, *87*, 156801.
9. Aumer, M. E.; LeBoeuf, S. F.; Moody, B. F.; Bedair, S. M. Strain-Induced Piezoelectric Field Effects on Light Emission Energy and Intensity from AlInGaN/InGaN Quantum Wells. *Appl. Phys. Lett.* **2001**, *79*, 3803–3805.
10. Azuhata, T.; Homma, T.; Ishikawa, Y.; Chichibu, S. F.; Sota, T.; Mukai, T. Current-Modulated Electroluminescence Spectroscopy and Its Application to InGaN Single-Quantum-Well Blue and Green Light-Emitting Diodes. *Appl. Phys. Lett.* **2001**, *79*, 1100–1102.

11. Bai, J.; Wang, T.; Sakai, S. Study of the Strain Relaxation in InGaN/GaN Multiple Quantum Well Structures. *J. Appl. Phys.* **2001**, *90*, 1740–1744.
12. Choi, C. K.; Kwon, Y. H.; Little, B. D.; Gainer, G. H.; Song, J. J.; Chang, Y. C.; Keller, S.; Mishra, U. K.; DenBaars, S. P. Time-Resolved Photoluminescence of $In_xGa_{1-x}N$/GaN Multiple Quantum Well Structures: Effect of Si Doping in the Barriers. *Phys. Rev. B* **2001**, *64*, 245339.
13. Kim, Y. W.; Suh, E. K.; Lee, H. J. Dislocation Behavior in InGaN/GaN Multi-Quantum-Well Structure Grown by Metalorganic Chemical Vapor Deposition. *Appl. Phys. Lett.* **2002**, *80*, 3949–3951.
14. Kuo, Y. H.; Lee, Y. K.; Ge, Y. S.; Ren, S.; Roth, J. E.; Kamins, T. I.; Miller, D. A. B.; Harris, J. S. Strong Quantum-Confined Stark Effect in Germanium Quantum-Well Structures on Silicon. *Nature* **2005**, *437*, 1334–1336.
15. Achermann, M.; Petruska, M. A.; Kos, S.; Smith, D. L.; Koleske, D. D.; Klimov, V. I. Energy-Transfer Pumping of Semiconductor Nanocrystals Using an Epitaxial Quantum Well. *Nature* **2004**, *429*, 642–646.
16. Teran, F. J.; Potemski, M.; Maude, D. K.; Andrearczyk, T.; Jaroszynski, J.; Karczewski, G. Pauli Paramagnetism and Landau Level Crossing in a Modulation Doped CdMnTe/CdMgTe Quantum Well. *Phys. Rev. Lett.* **2002**, *88*, 186803.
17. Yang, J.; Son, J. S.; Yu, J. H.; Joo, J.; Hyeon, T. Advances in the Colloidal Synthesis of Two-Dimensional Semiconductor Nanoribbons. *Chem. Mater.* **2013**, *25*, 1190–1198.
18. Fainblat, R.; Frohleiks, J.; Muckel, F.; Yu, J. H.; Yang, J.; Hyeon, T.; Bacher, G. Quantum Confinement-Controlled Exchange Coupling in Manganese(II)-Doped CdSe Two-Dimensional Quantum Well Nanoribbons. *Nano Lett.* **2012**, *12*, 5311–5317.
19. Yu, J. H.; Liu, X. Y.; Kweon, K. E.; Joo, J.; Park, J.; Ko, K. T.; Lee, D.; Shen, S. P.; Tivakornsasithorn, K.; Son, J. S.; *et al.* Giant Zeeman Splitting in Nucleation-Controlled Doped CdSe: Mn^{2+} Quantum Nanoribbons. *Nat. Mater.* **2010**, *9*, 47–53.
20. Son, J. S.; Wen, X. D.; Joo, J.; Chae, J.; Baek, S. I.; Park, K.; Kim, J. H.; An, K.; Yu, J. H.; Kwon, S. G.; *et al.* Large-Scale Soft Colloidal Template Synthesis of 1.4 nm Thick CdSe Nanosheets. *Angew. Chem., Int. Ed.* **2009**, *48*, 6861–6864.
21. Tessier, M. D.; Biadala, L.; Bouet, C.; Ithurria, S.; Abecassis, B.; Dubertret, B. Phonon Line Emission Revealed by Self-Assembly of Colloidal Nanoplatelets. *ACS Nano* **2013**, *7*, 3332–3340.
22. Tessier, M. D.; Javaux, C.; Maksimovic, I.; Loriette, V.; Dubertret, B. Spectroscopy of Single CdSe Nanoplatelets. *ACS Nano* **2012**, *6*, 6751–6758.
23. Mahler, B.; Nadal, B.; Bouet, C.; Patriarche, G.; Dubertret, B. Core/Shell Colloidal Semiconductor Nanoplatelets. *J. Am. Chem. Soc.* **2012**, *134*, 18591–18598.
24. Son, J. S.; Yu, J. H.; Kwon, S. G.; Lee, J.; Joo, J.; Hyeon, T. Colloidal Synthesis of Ultrathin Two-Dimensional Semiconductor Nanocrystals. *Adv. Mater.* **2011**, *23*, 3214–3219.
25. Gao, H. W.; Fu, A.; Andrews, S. C.; Yang, P. D. Cleaved-Coupled Nanowire Lasers. *Proc. Natl. Acad. Sci. U.S.A.* **2013**, *110*, 865–869.
26. Tang, J. Y.; Huo, Z. Y.; Brittman, S.; Gao, H. W.; Yang, P. D. Solution-Processed Core-Shell Nanowires for Efficient Photovoltaic Cells. *Nat. Nanotechnol.* **2011**, *6*, 568–572.
27. Hahn, C.; Zhang, Z. Y.; Fu, A.; Wu, C. H.; Hwang, Y. J.; Gargas, D. J.; Yang, P. D. Epitaxial Growth of InGaN Nanowire Arrays for Light Emitting Diodes. *ACS Nano* **2011**, *5*, 3970–3976.
28. Gargas, D. J.; Gao, H. W.; Wang, H. T.; Yang, P. D. High Quantum Efficiency of Band-Edge Emission from ZnO Nanowires. *Nano Lett.* **2011**, *11*, 3792–3796.
29. Yan, R. X.; Gargas, D.; Yang, P. D. Nanowire Photonics. *Nat. Photonics* **2009**, *3*, 569–576.
30. Yang, P. D.; Wirnsberger, G.; Huang, H. C.; Cordero, S. R.; McGehee, M. D.; Scott, B.; Deng, T.; Whitesides, G. M.; Chmelka, B. F.; Buratto, S. K.; *et al.* Mirrorless Lasing from Mesostructured Waveguides Patterned by Soft Lithography. *Science* **2000**, *287*, 465–467.
31. Yang, P. D.; Lieber, C. M. Nanorod-Superconductor Composites: A Pathway to Materials with High Critical Current Densities. *Science* **1996**, *273*, 1836–1840.
32. Huang, M. H.; Mao, S.; Feick, H.; Yan, H. Q.; Wu, Y. Y.; Kind, H.; Weber, E.; Russo, R.; Yang, P. D. Room-Temperature Ultraviolet Nanowire Nanolasers. *Science* **2001**, *292*, 1897–1899.
33. Zhong, Z. H.; Wang, D. L.; Cui, Y.; Bockrath, M. W.; Lieber, C. M. Nanowire Crossbar Arrays as Address Decoders for Integrated Nanosystems. *Science* **2003**, *302*, 1377–1379.
34. Huang, Y.; Duan, X. F.; Cui, Y.; Lauhon, L. J.; Kim, K. H.; Lieber, C. M. Logic Gates and Computation from Assembled Nanowire Building Blocks. *Science* **2001**, *294*, 1313–1317.
35. Cui, Y.; Lieber, C. M. Functional Nanoscale Electronic Devices Assembled Using Silicon Nanowire Building Blocks. *Science* **2001**, *291*, 851–853.
36. Yao, J.; Yan, H.; Lieber, C. M. A Nanoscale Combing Technique for the Large-Scale Assembly of Highly Aligned Nanowires. *Nat. Nanotechnol.* **2013**, *8*, 329–335.
37. Yan, K. Y.; Zhang, L. X.; Qiu, J. H.; Qiu, Y. C.; Zhu, Z. L.; Wang, J. N.; Yang, S. H. A Quasi-Quantum Well Sensitized Solar Cell with Accelerated Charge Separation and Collection. *J. Am. Chem. Soc.* **2013**, *135*, 9531–9539.
38. Qiu, Y. F.; Yang, S. H. ZnO Nanotetrapods: Controlled Vapor-Phase Synthesis and Application for Humidity Sensing. *Adv. Funct. Mater.* **2007**, *17*, 1345–1352.
39. Guo, Y. J.; Alvarado, S. R.; Barclay, J. D.; Vela, J. Shape-Programmed Nanofabrication: Understanding the Reactivity of Dichalcogenide Precursors. *ACS Nano* **2013**, *7*, 3616–3626.
40. Ruberu, T. P. A.; Albright, H. R.; Callis, B.; Ward, B.; Cisneros, J.; Fan, H. J.; Vela, J. Molecular Control of the Nanoscale: Effect of Phosphine-Chalcogenide Reactivity on CdS-CdSe Nanocrystal Composition and Morphology. *ACS Nano* **2012**, *6*, 5348–5359.
41. Ruberu, T. P. A.; Vela, J. Expanding the One-Dimensional CdS-CdSe Composition Landscape: Axially Anisotropic $CdS_{1-x}Se_x$ Nanorods. *ACS Nano* **2011**, *5*, 5775–5784.
42. Li, J. J.; Wang, Y. A.; Guo, W. Z.; Keay, J. C.; Mishima, T. D.; Johnson, M. B.; Peng, X. G. Large-Scale Synthesis of Nearly Monodisperse CdSe/CdS Core/Shell Nanocrystals Using Air-Stable Reagents *via* Successive Ion Layer Adsorption and Reaction. *J. Am. Chem. Soc.* **2003**, *125*, 12567–12575.
43. Chen, Y.; Vela, J.; Htoon, H.; Casson, J. L.; Werder, D. J.; Bussian, D. A.; Klimov, V. I.; Hollingsworth, J. A. "Giant" Multishell CdSe Nanocrystal Quantum Dots with Suppressed Blinking. *J. Am. Chem. Soc.* **2008**, *130*, 5026–5027.
44. Malko, A. V.; Park, Y. S.; Sampat, S.; Galland, C.; Vela, J.; Chen, Y. F.; Hollingsworth, J. A.; Klimov, V. I.; Htoon, H. Pump-Intensity- and Shell-Thickness-Dependent Evolution of Photoluminescence Blinking in Individual Core/Shell CdSe/CdS Nanocrystals. *Nano Lett.* **2011**, *11*, 5213–5218.
45. Guo, W. H.; Li, J. J.; Wang, Y. A.; Peng, X. G. Luminescent CdSe/CdS Core/Shell Nanocrystals in Dendron Boxes: Superior Chemical, Photochemical and Thermal Stability. *J. Am. Chem. Soc.* **2003**, *125*, 3901–3909.
46. Battaglia, D.; Li, J. J.; Wang, Y. J.; Peng, X. G. Colloidal Two-Dimensional Systems: CdSe Quantum Shells and Wells. *Angew. Chem., Int. Ed.* **2003**, *42*, 5035–5039.
47. Ghosh, Y.; Mangum, B. D.; Casson, J. L.; Williams, D. J.; Htoon, H.; Hollingsworth, J. A. New Insights into the Complexities of Shell Growth and the Strong Influence of Particle Volume in Nonblinking "Giant" Core/Shell Nanocrystal Quantum Dots. *J. Am. Chem. Soc.* **2012**, *134*, 9634–9643.
48. Yin, Y. D.; Rioux, R. M.; Erdonmez, C. K.; Hughes, S.; Somorjai, G. A.; Alivisatos, A. P. Formation of Hollow Nanocrystals through the Nanoscale Kirkendall Effect. *Science* **2004**, *304*, 711–714.
49. Javaux, C.; Mahler, B.; Dubertret, B.; Shabaev, A.; Rodina, A. V.; Efros, A. L.; Yakovlev, D. R.; Liu, F.; Bayer, M.; Camps, G.; *et al.* Thermal Activation of Non-radiative Auger Recombination in Charged Colloidal Nanocrystals. *Nat. Nanotechnol.* **2013**, *8*, 206–212.
50. Chen, R.; Ye, Q. L.; He, T. C.; Ta, V. D.; Ying, Y. J.; Tay, Y. Y.; Wu, T.; Sun, H. D. Exciton Localization and Optical Properties Improvement in Nanocrystal-Embedded ZnO Core-Shell Nanowires. *Nano Lett.* **2013**, *13*, 734–739.

51. Jones, M.; Lo, S. S.; Scholes, G. D. Quantitative Modeling of the Role of Surface Traps in CdSe/CdS/ZnS Nanocrystal Photoluminescence Decay Dynamics. *Proc. Natl. Acad. Sci. U.S.A.* **2009**, *106*, 3011–3016.
52. Afshar, M.; Sadewasser, S.; Albert, J.; Lehmann, S.; Abou-Ras, D.; Marron, D. F.; Rockett, A. A.; Rasanen, E.; Lux-Steiner, M. C. Chalcopyrite Semiconductors for Quantum Well Solar Cells. *Adv. Energy Mater.* **2011**, *1*, 1109–1115.
53. Xu, J.; Yang, X.; Wang, H. K.; Chen, X.; Luan, C. Y.; Xu, Z. X.; Lu, Z. Z.; Roy, V. A. L.; Zhang, W. J.; Lee, C. S. Arrays of $ZnO/Zn_xCd_{1-x}Se$ Nanocables: Band Gap Engineering and Photovoltaic Applications. *Nano Lett.* **2011**, *11*, 4138–4143.
54. Giri, P. K.; Kesavamoorthy, R.; Panigrahi, B. K.; Nair, K. G. M. Evidence for Fast Decay Dynamics of the Photoluminescence from Ge Nanocrystals Embedded in SiO_2. *Solid State Commun.* **2005**, *133*, 229–234.
55. Sagarzazu, G.; Inoue, K.; Saruyama, M.; Sakamoto, M.; Teranishi, T.; Masuo, S.; Tamai, N. Ultrafast Dynamics and Single Particle Spectroscopy of Au-CdSe Nanorods. *Phys. Chem. Chem. Phys.* **2013**, *15*, 2141–2152.
56. Marceddu, M.; Saba, M.; Quochi, F.; Lai, A.; Huang, J.; Talapin, D. V.; Mura, A.; Bongiovanni, G. Charged Excitons, Auger Recombination and Optical Gain in CdSe/CdS Nanocrystals. *Nanotechnology* **2012**, *23*, 015201.
57. Wang, K.; Chen, J. J.; Zhou, W. L.; Zhang, Y.; Yan, Y. F.; Pern, J.; Mascarenhas, A. Direct Growth of Highly Mismatched Type II ZnO/ZnSe Core/Shell Nanowire Arrays on Transparent Conducting Oxide Substrates for Solar Cell Applications. *Adv. Mater.* **2008**, *20*, 3248–3253.
58. Xu, J.; Yang, X.; Wang, H. K.; Chen, X.; Luan, C. Y.; Xu, Z. X.; Lu, Z. Z.; Roy, V. A. L.; Zhang, W. J.; Lee, C. S. Arrays of $ZnO/Zn_xCd_{1-x}Se$ Nanocables: Band Gap Engineering and Photovoltaic Applications. *Nano Lett.* **2011**, *11*, 4138–4143.